Journal of Nuclear Materials 392 (2009) 464–470

Contents lists available at ScienceDirect

Journal of Nuclear Materials

journal homepage: www.elsevier.com/locate/jnucmat

Thermal transport properties of hafnium hydrides and deuterides

B. Tsuchiya [a,*], Y. Arita [b], H. Muta [c], K. Kurosaki [c], K. Konashi [a], S. Nagata [a], T. Shikama [a]

[a] Institute for Materials Research, Tohoku University, 2-1-1, Katahira, Aoba-ku, Sendai 980-8577, Japan
[b] EcoTopia Science Institute, Nagoya University, Nagoya 464-8603, Japan
[c] Department of Nuclear Engineering, Graduate School of Engineering, Osaka University, 2-1, Yamadaoka, Osaka 565-0871, Japan

ARTICLE INFO

Article history:
Received 30 September 2008
Accepted 13 April 2009

PACS:
05.70.Fh
72.15.Ed
66.30.Xj

ABSTRACT

The thermal conductivities of δ′-, δ-, δ+ε-, and ε-phase hafnium hydrides and deuterides with various hydrogen isotope concentrations (HfH_x, $1.48 \leqslant x \leqslant 2.03$; HfD_x, $1.55 \leqslant x \leqslant 1.94$) were evaluated within the temperature range of 290–570 K from the measured thermal diffusivity, calculated specific heat, and density. The thermal conductivities of δ′-, δ-, δ+ε-, and ε-phase HfH_x and HfD_x are independent of the temperature within the range 300–550 K and are in the range 0.15–0.22 W/cm K and 0.17–0.23 W/cm K, respectively; these values are similar to and lower than the observed thermal conductivities of α-phase Hf. The experimental results for the electrical resistivities of δ′-, δ-, δ+ε-, and ε-phase HfH_x and HfD_x and the Lorenz number corresponding to the electronic conduction, obtained from the Wiedemann–Franz rule, indicated that heat conduction due to electron migration significantly influences the thermal conductivity values at high temperatures. On the other hand, heat conduction due to phonon migration significantly affects the isotope effects on the thermal transport properties.

1. Introduction

Hafnium hydride (HfH_x) and deuteride (HfD_x) could be used to fabricate one of the control rods for fast-neutron flux in fast reactors [1]. These materials are found suitable for this purpose because the transition metal hafnium (Hf) strongly absorbs thermal neutrons [2], which are generated by the elastic collision of fast neutrons with the hydrogen atoms occupying the tetrahedral interstitial sites of HfH_x and HfD_x [3], and does not generate certain gases such as ^{4}He during the nuclear reaction. However, the concentration of hydrogen in HfH_x and HfD_x ($x > 1.5$) decreases due to the decomposition of HfH_x and HfD_x at temperatures above 623 K and elastic collisions with fast neutrons. Therefore, it is extremely important to understand the changes in the physical, chemical, thermal, and mechanical properties of HfH_x and HfD_x with hydrogen distribution within the control rod.

In the present study, we investigated the thermal diffusivity, specific heat, and thermal conductivity of HfH_x and HfD_x ($1.48 \leqslant x \leqslant 2.03$); these are some of the most important parameters representing the thermal properties. The temperature at the control rods in fast reactors is speculated to be in the range of approximately 673–873 K; this temperature significantly depends on the temperatures of the cooling materials made from liquid sodium (Na). In this study, annealing was carried out over a wide range of temperatures (290–570 K). Furthermore, the hydrogen isotope effects as well as the thermal transport properties pertaining to the migration of free electrons and phonons in HfH_x and HfD_x with various compositions are investigated by considering the thermal conductivity, experimental data on electrical resistivity, and the Wiedemann–Franz rule.

2. Experiments

HfH_x and HfD_x compounds with hydrogen composition in the range of $1.48 \leqslant x \leqslant 2.03$ were prepared using a Sieverts apparatus by heating and outgassing hafnium metal including impurities such as Zr (6.3 at.%), C (<0.04 at.%), and O (<0.0002 at.%), the concentrations of which were determined through chemical analysis, in an evacuated quartz tube at 1073 K. Subsequently, the hafnium metal was exposed to hydrogen gas (99.9% pure) in the tube at pressures ranging from 0.1×10^5 to 1.0×10^5 Pa for 4 h. The specimens were then cooled to room temperature at a rate of 4.5×10^{-3} K/s while still in the tube. The compositions of the specimens were calculated on the basis of the mass gain caused by hydrogenation.

Fig. 1 shows the X-ray diffraction (XRD) patterns for α-Hf, δ′-$HfH_{1.48}$, δ′-$HfH_{1.57}$, δ-$HfH_{1.70}$, δ+ε-$HfH_{1.76}$, ε-$HfH_{1.88}$, and ε-$HfH_{2.02}$ at room temperature. The crystal structures of the samples with $1.60 < x \leqslant 1.75$ and $1.84 < x \leqslant 2.03$ are face-centered cubic (fcc) δ-phase and face-centered tetragonal (fct) ε-phase, respectively [3–5]. HfH_x samples with $1.75 < x \leqslant 1.84$ have δ+ε-phase structures that comprise a mixture of the δ-phase and the ε-phase. The crystal structures of the samples with $1.48 \leqslant x \leqslant 1.60$ are distinguishable

* Corresponding author. Tel.: +81 22 215 2063; fax: +81 22 215 2061.
E-mail address: tsuchiya@imr.tohoku.ac.jp (B. Tsuchiya).

0022-3115/$ - see front matter © 2009 Elsevier B.V. All rights reserved.
doi:10.1016/j.jnucmat.2009.04.009

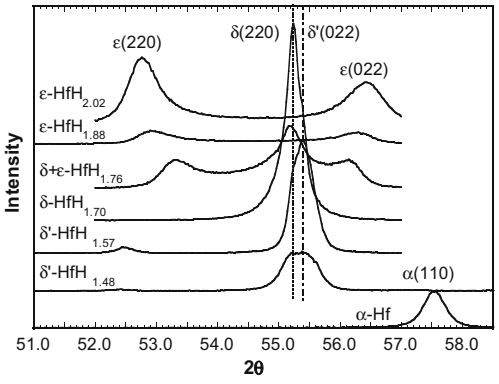

Fig. 1. XRD patterns for α-Hf, δ′-$HfH_{1.48}$, δ′-$HfH_{1.57}$, δ-$HfH_{1.70}$, δ+ε-$HfH_{1.76}$, ε-$HfH_{1.88}$, and ε-$HfH_{2.02}$ at room temperature.

from the δ-phase structure by using the XRD patterns, as shown in Fig. 1; these samples exhibit a pseudocubic defective δ-phase (δ′-phase) that has previously been reported in literature [5–7]. The unit cell of this pseudocubic phase is slightly deformed and displays some tetragonal characteristics; for example, the lattice constants for the *a*- and *b*-axes for the δ′-phase are identical to those for the δ-phase, while that for the *c*-axis for the δ′-phase is lower than that for the δ-phase. The diffraction patterns obtained from transmission electron microscopy (TEM) observations and XRD measurements performed while annealing the samples up to 673 K revealed that the deformed cubic phase for δ′-$HfH_{1.52}$ is converted into an fcc phase at temperatures above 353 K. In this study, the tetragonal phase was observed for $HfH_{1.48-1.60}$. It has been reported [3] that the hydrogen atoms occupy the vacant tetrahedral interstices in the ε- and δ-phases. The scanning electron micrographs confirmed that the lattice expansion caused by the occupation of the interstitial spaces by the hydrogen atoms led to the formation of microcracks in the HfH_x and HfD_x samples with $x \geqslant 1.88$. Fig. 2 shows the theoretical densities of δ′-, δ-, δ+ε-, and ε-phase HfH_x and HfD_x ($1.48 \leqslant x \leqslant 2.03$) and α-Hf at room temperature, where ● and △ denote the reference data for HfH_x and α-Hf, respectively [8], and ♦ and ▽ represent the experimental data obtained in this study for HfH_x and HfD_x, respectively; the data are obtained on the basis of the weight and volume of the samples. As can be seen in Fig. 2, the theoretical densities of HfH_x and HfD_x d_{HfHx} and d_{HfDx} are dependent on *x*; the relationships between *x* ($1.48 \leqslant x \leqslant 2.03$) and the theoretical densities [g/cm^3] are

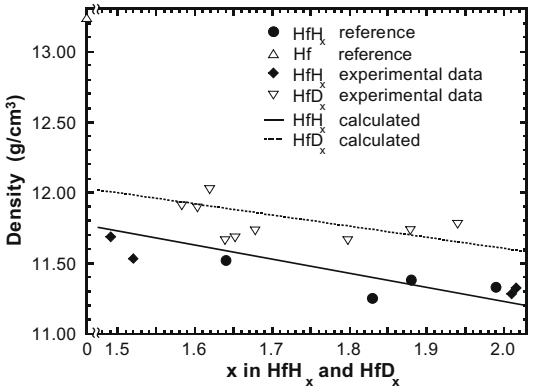

Fig. 2. Theoretical densities of δ′-, δ-, δ+ε-, and ε-phase HfH_x and HfD_x ($1.48 \leqslant x \leqslant 2.03$) with various compositions and α-Hf at room temperature. ● and △ are obtained from the Ref. [8]. ♦ and ▽ represent the data obtained in this study. The solid and dotted lines represent the calculated theoretical densities of HfH_x and HfD_x, respectively, which are dependent on the composition.

assumed to be as follows: $d_{HfHx} = d_{Hf} - 1.01x$ and $d_{HfDx} = d_{Hf} - 0.82x$, where d_{Hf} represents the theoretical density of metallic α-Hf (13.24 g/cm^3) [8]. The theoretical densities d_{HfHx} and d_{HfDx} calculated using these equations are represented by HfH_x calc. (—) and HfD_x calc. (·····), respectively, in Fig. 2.

Thermal diffusivity measurements were carried out on samples (ϕ: 10.0 mm; height: 1.0 mm) by using a laser-flash method [9]. This method enables the investigation of the thermal properties of simple systems. The measurements were carried out while heating the samples up to approximately 570 K and subsequently cooling them down to room temperature in vacuum. The maximum temperature was set to 570 K because HfH_x and HfD_x rapidly decompose at temperatures above 600 K. In the temperature range of 290–570 K, several phases of the HfH_x and HfD_x remained stable. One exception to this is the Hf-rich tetragonal compound with the δ′-phase, which approaches δ-phase cubic symmetry at temperatures of approximately 358–373 K [6,7].

In order to determine the thermal conductivities for HfH_x and HfD_x samples with different phases, the specific heat of a δ′-$HfH_{1.53}$ sample (size: $1.0 \times 1.0 \times 20.0$ mm^3) and δ′-$HfH_{1.57}$ and δ+ε-$HfD_{1.76}$ samples (size: $1.0 \times 1.0 \times 2.0$ mm^3) was measured from room temperature to approximately 573 K using a direct heating pulse calorimeter (DHPC) at Nagoya Univ. [10,11] and a differential scanning calorimeter (DSC) at Osaka Univ. [12]. The data obtained from the DSC measurements were calibrated by considering the specific heat of sapphire (α-Al_2O_3) as the standard value.

The changes in the thermal conductivity values with the composition and temperatures can be mainly attributed to phonon and electron scattering caused by the presence of vacancies between the hydrogen atoms at the tetrahedral interstitial sites and the interface between different phase structures as well as the thermal vibration of the constitutive atoms. To investigate the electronic conduction corresponding to thermal transport, the electrical resistivity of specimens (size: $1.0 \times 1.0 \times 20.0$ mm^3) was measured using a four-contact DC method [13]. The measurements were performed while heating the samples up to approximately 570 K in vacuum.

3. Experimental results

Fig. 3(a)–(h) shows the thermal diffusivities of ε-phase $HfH_{1.88-2.01}$, δ+ε-phase $HfH_{1.76-1.83}$, δ-phase $HfH_{1.63-1.75}$, δ′-phase $HfH_{1.48-1.60}$, ε-phase $HfD_{1.88-1.94}$, δ+ε-phase $HfD_{1.78-1.84}$, δ-phase $HfD_{1.64-1.68}$, and δ′-phase $HfD_{1.55-1.60}$, respectively, as a function of temperatures in the range of 290–570 K, where ●, ▲, ♦, and ▼ represent the data collected while heating the samples, and ○, △, ◇, and ▽ represent the data collected while cooling the samples. The dotted curves in Fig. 3(b) and (f) represent the thermal diffusivity of α-Hf, which has been reported previously [14]. The agreement between the heating and cooling curves indicates that the hydrogen concentration of the samples does not reduce due to thermal desorption when the samples are being heated to 570 K. The thermal diffusivities of HfH_x at all temperatures and hydrogen concentrations are higher than those of HfD_x, in that, isotope effects exist. For ε-phase HfH_x and HfD_x, the thermal diffusivities increase as the value of *x* approaches 2.0, that is, as a stoichiometric structure is attained. Moreover, the thermal diffusivities decrease with an increase in temperature because of the effects of thermal vibration during heat conduction caused by the migration of carriers such as phonons and electrons. A similar trend has been observed in ε-phase ZrH_x and ZrD_x [15]. The existence of microcracks in the ε-HfH_x and ε-HfD_x samples has no influence on the thermal diffusivity. Additionally, the thermal diffusivities of δ+ε-phase HfH_x and HfD_x hardly change with the

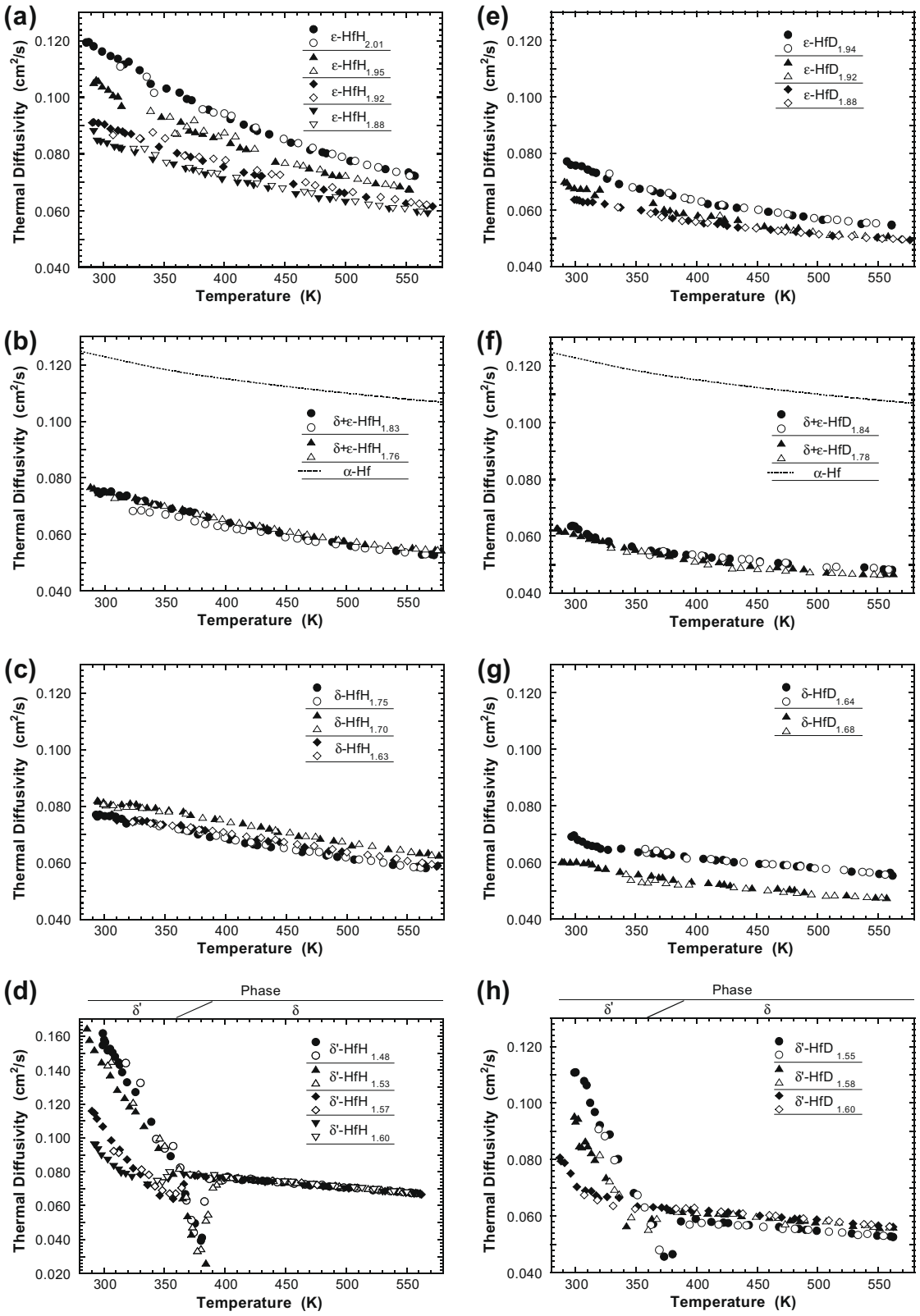

Fig. 3. Temperature dependence of the thermal diffusivities of (a) ε-$HfH_{1.88–2.01}$, (b) δ+ε-$HfH_{1.76–1.83}$ and α-Hf, (c) δ-$HfH_{1.63–1.75}$, (d) δ′-$HfH_{1.48–1.60}$, (e) ε-$HfD_{1.88–1.94}$, (f) δ+ε-$HfD_{1.78–1.84}$ and α-Hf, (g) δ-$HfD_{1.64–1.68}$, and (h) δ′-$HfD_{1.55–1.60}$.

composition; however, they decrease with an increase in temperature. The total thermal diffusivities at various temperatures are the lowest for δ′-, δ-, and ε-phase HfH_x and HfD_x, and α-Hf. For δ′-phase HfH_x and HfD_x, the thermal diffusivity decreases rapidly in the temperature range of 320–380 K, thereafter increases rapidly, and eventually decreases gradually as the temperature reaches 570 K. The thermal diffusivity values of δ′-phase HfH_x and HfD_x at temperatures above 350–390 K are similar to those

of δ-phase HfH_x and HfD_x. This is due to the phase transformation from the δ′-phase structure to the δ-phase structure. Moreover, the migration of hafnium atoms in the lattice cell of the hydride significantly influences the change in the thermal diffusivity of the δ′-phase compounds.

In order to demonstrate in more detail the effects of phase transformation on the thermal diffusivities, the change in the thermal diffusivities of $HfH_{1.48-2.03}$ and $HfD_{1.55-1.94}$ at 300, 350, 400, 450, 500, and 550 K with the composition of the compounds is plotted in Fig. 4(a) and (b). It should be noted that the data points at temperatures above 400 K for $x = 1.48–1.60$ correspond to the δ-phase compounds. The thermal diffusivities of $HfH_{1.48-1.53}$ at 300 K are higher than that of α-Hf. Furthermore, the thermal diffusivities of $HfH_{1.48-2.03}$ and $HfD_{1.55-1.94}$ at temperatures above 400 K are almost constant and are in the ranges 0.05–0.09 cm^2/s and 0.045–0.06 cm^2/s, respectively; these values are approximately half of the thermal diffusivity of α-Hf under the same conditions. The thermal diffusivities of HfH_x decrease for $x > 2.0$ because of the effect of the hydrogen atoms occupying the octahedral as well as the vacant tetrahedral interstices.

Fig. 5 shows the specific heat of α-Hf, which has been reported in [16], the specific heat of δ′-$HfH_{1.53}$, which was measured using the DHPC, the specific heat of δ′-$HfH_{1.57}$ and δ+ε-$HfD_{1.76}$, the values of which were measured using the DSC, in the temperature range of 300–570 K. The values of specific heat at several different compositions and temperatures are very similar; further, the values indicate the isotope effects. The λ-type peaks in the spectra indicate the rapid heat absorption due to the phase transformation from δ′ to δ in the temperature range of 360–380 K. The experimental data are in agreement with previously reported data [10]. However, the experimental values are scattered and cannot be accurately interpolated to obtain the data pertaining to compounds with different compositions. In the present study, the specific heat values of HfH_x and HfD_x ($1.60 < x \leqslant 2.03$) Cp^{HfHx} and Cp^{HfDx}, which are represented by HfH_x calc. (·····) and HfD_x calc. (–···–) in Fig. 5, are estimated by considering the previously reported values of specific heat Cp^{Hf}, Cp^{Zr}, and Cp^{ZrHx} for Hf, Zr, $ZrH_{1.58}$, $ZrH_{2.00}$, $ZrD_{1.58}$, and $ZrD_{2.00}$. The $Cp^{HfH(D)x}$ value, which is the specific heat of $HfH(D)_x$, can be expressed as a function of temperature T as $Cp^{HfH(D)x} = Cp^{ZrH(D)x} \times Cp^{Hf}/Cp^{Zr} = 0.0940 + 3.30 \times 10^{-4}T$ for $1.60 < x \leqslant 2.03$; here, Cp^{Hf}, Cp^{Zr}, and $Cp^{ZrH(D)x}$ (J/g K) can be expressed as $Cp^{Hf} = 0.130 + 4.64 \times 10^{-5}T$, $Cp^{Zr} = 0.235 + 1.49 \times 10^{-4}T$ ($290\ K \leqslant T \leqslant 570\ K$) [16], $Cp^{ZrHx} = 0.155 + 7.52 \times 10^{-4}T$, and $Cp^{ZrDx} = Cp^{ZrHx} \times 1.27$, respectively [17–19]. Using the experimental data, the Cp^{HfHx} and Cp^{HfDx} values of δ′-HfH_x and δ′-HfD_x ($1.48 \leqslant x \leqslant 1.60$), represented by HfH_x calc. (—) and HfD_x calc. (–·–) in Fig. 5, can be expressed as $Cp^{HfHx} = -0.917 + 6.00 \times 10^{-3}T - 1.04 \times 10^{-5}T^2 + 6.24 \times 10^{-9}T^3$ and $Cp^{HfDx} = Cp^{HfHx} \times 1.27$, respectively. However, the values of specific heat at the phase-transition temperature are not considered for obtaining the equations.

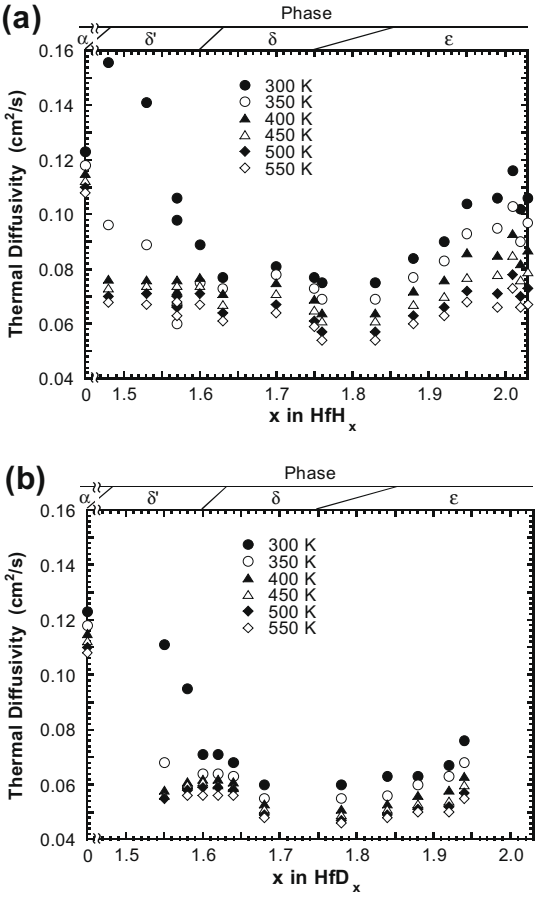

Fig. 4. Dependence of the thermal diffusivities of (a) HfH_x and (b) HfD_x on the composition at temperatures of 300, 350, 400, 450, 500, and 550 K.

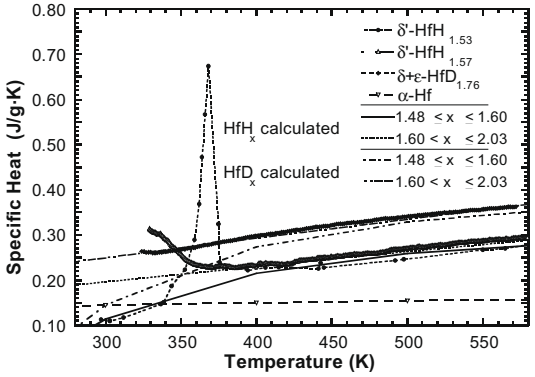

Fig. 5. Temperature dependence of the specific heat of α-Hf at different temperatures (these values have been previously reported in [16]) and the specific heat of δ′-$HfH_{1.53}$, δ′-$HfH_{1.57}$, and δ+ε-$HfD_{1.76}$ (determined in the present study). The lines — and ····· represent the calculated specific heat of $HfH_{1.48 \leqslant x \leqslant 1.60}$ and $HfH_{1.60 < x \leqslant 2.03}$, respectively; the calculated specific heat is dependent on the temperature. The lines –·– and –···– represent the calculated specific heat of $HfD_{1.48 \leqslant x \leqslant 1.60}$ and $HfD_{1.60 < x \leqslant 2.03}$, respectively; these values are dependent on the temperature.

4. Discussion

Fig. 6(a) and (b) shows a comparison of the thermal conductivities for δ′-$HfH_{1.53}$, δ-$HfH_{1.63}$, δ+ε-$HfH_{1.83}$, ε-$HfH_{1.92}$, δ′-$HfD_{1.55}$, δ-$HfD_{1.64}$, δ+ε-$HfD_{1.84}$, and ε-$HfD_{1.92}$ with the thermal conductivity values previously reported for α-Hf [20]. The thermal conductivities λ_i, where i = HfH_x, HfD_x, and Hf, can be expressed as $\lambda_i = \alpha_i Cp^i d_i$, where α_i, Cp^i, and d_i are the measured thermal diffusivity, the calculated specific heat, and density of i, respectively. However, the thermal diffusivity data pertaining to the transition from the δ′-phase to the δ-phase in the temperature range of 365–390 K are eliminated while formulating this equation. The thermal conductivities of HfH_x at several compositions, temperatures, and phases are slightly lower than those for HfD_x. At 550 K, the conductivities for HfH_x and HfD_x are in the ranges 0.17–0.22 W/cm K and 0.20–0.23 W/cm K, respectively; these values are similar to the thermal conductivity of α-Hf (0.21 W/cm K) [20].

Fig. 7(a) and (b) shows the electrical resistivities of α-Hf, δ′-$HfH_{1.53}$, δ-$HfH_{1.63}$, δ+ε-$HfH_{1.81}$, ε-$HfH_{1.92}$ and those of δ′-$HfD_{1.55}$, δ-$HfD_{1.64}$, δ+ε-$HfD_{1.78}$, and ε-$HfD_{1.92}$, respectively, in the temperature range of 290–570 K. A comparison of Fig. 7(a) and (b) did

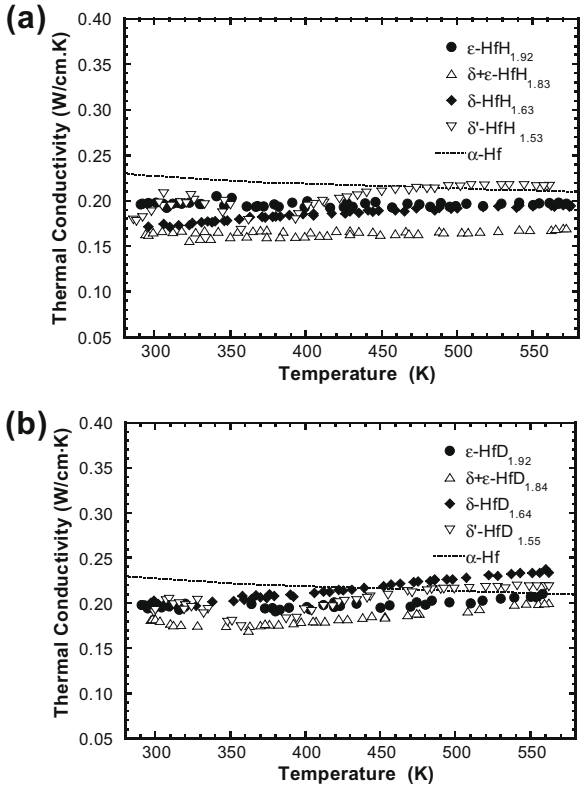

Fig. 6. Temperature dependence of the thermal conductivities of (a) α-Hf, δ′-$HfH_{1.53}$, δ-$HfH_{1.63}$, δ+ε-$HfH_{1.83}$, and ε-$HfH_{1.92}$, and (b) α-Hf, δ′-$HfD_{1.55}$, δ-$HfD_{1.64}$, δ+ε-$HfD_{1.84}$, and ε-$HfD_{1.92}$.

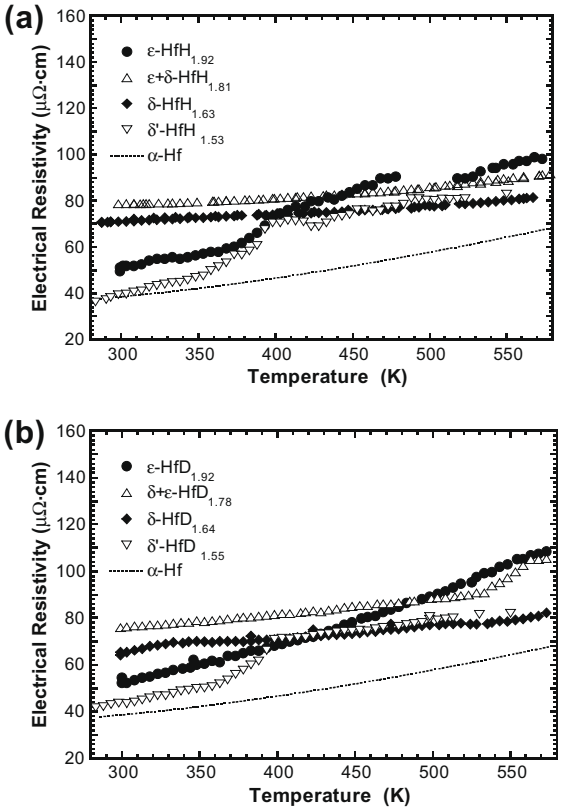

Fig. 7. Temperature dependence of the electrical resistivities of (a) α-Hf, δ′-$HfH_{1.53}$, δ-$HfH_{1.63}$, δ+ε-$HfH_{1.81}$, and ε-$HfH_{1.92}$, and (b) α-Hf, δ′-$HfD_{1.55}$, δ-$HfD_{1.64}$, δ+ε-$HfD_{1.78}$, and ε-$HfD_{1.92}$.

not reveal any isotope effects, regardless of the different compositions of each phase considered. The electrical resistivity of δ′-phase $HfH_{1.53}$ increase rapidly at the phase-transition temperature below 400 K, as do the thermal diffusivity and the specific heat, and thereafter increases gradually due to electron–phonon scattering by acoustic and optical modes. For compounds in other phases, the resistivities increase gradually, although the rate at which the resistivities increase for ε-phase compounds is different from that for δ-phase and δ+ε-phase compounds. The thermal conductivities of ε-$HfH_{1.92}$, δ+ε-$HfH_{1.83}$, δ-$HfH_{1.63}$, δ′-$HfH_{1.53}$, ε-$HfD_{1.92}$, δ+ε-$HfD_{1.84}$, δ-$HfD_{1.64}$, δ′-$HfD_{1.55}$, and α-Hf were estimated using the values of electronic conduction (λ_e^i) obtained from the relation $\lambda_e^i = L_e^i \sigma_i T$, which is based on the Wiedemann–Franz rule, as shown in Fig. 8(a)–(i). In the abovementioned equation, σ_i denotes the electrical conductivity of i and is obtained from the measured electrical resistivity ρ_i ($\sigma_i = 1/\rho_i$), although the composition considered for each phase is different. Further, L_e^i is the Lorenz number corresponding to the electronic conduction in i, i.e., $L_e^i = (\pi^2/3)(k_B/e)^2 \approx 2.45 \times 10^{-8}\ W\Omega/K^2$, where k_B and e are the Boltzmann constant and the elementary electric charge, respectively. Finally, the thermal conductivities of ε-$HfH_{1.92}$, δ+ε-$HfH_{1.83}$, δ-$HfH_{1.63}$, δ′-$HfH_{1.53}$, ε-$HfD_{1.92}$, δ+ε-$HfD_{1.84}$, δ-$HfD_{1.64}$, δ′-$HfD_{1.55}$, and α-Hf associated with phonon conduction λ_p^i were determined by subtracting λ_e^i from the calculated thermal conductivity λ^i (i.e., $\lambda^i = \lambda_e^i + \lambda_p^i$), as shown in Fig. 8(a)–(i). Heat is conducted for each phase at 300–550 K because of the migration of both free electrons and phonons, while heat is conducted for α-phase at temperatures above 450 K because of the migration of free electrons only. At high temperatures near 550 K, the contribution of the migration of electrons to heat conduction is greater than that of the migration of phonons. In δ′-phase compounds, electron migration significantly dominates the heat conduction at temperatures below 400 K. The dependence of the thermal diffusivity of δ-, δ+ε-, and ε-phase compounds on the composition indicates that phonon scattering by electrons and phonons has a significant effect on the nonstoichiometric structures; this is consistent with previously reported results for ε-phase $ZrH_{1.76-2.03}$ and δ-phase $TiH_{1.64-1.98}$ [13,21]. The lowest values of thermal diffusivity for δ+ε-phase HfH_x and HfD_x samples can be attributed to the effects of phonon and electron scattering at the interface between the δ- and ε-phases. The isotope effects on thermal diffusivities are ascribed to electron–phonon scattering by the optical mode and to phonon–phonon scattering. The difference in the λ_p^i values of HfH_x and HfD_x is slightly larger than the difference in λ_e^i. Therefore, phonon conduction has a stronger influence on the isotope effects on thermal transport properties.

5. Summary

The thermal diffusivity of HfH_x and HfD_x ($1.48 \leqslant x \leqslant 2.03$), prepared at different temperatures and hydrogen-gas pressures using the Sieverts apparatus, was measured for the temperature range from room temperature to 570 K by means of a laser-flash method. The thermal diffusivities of HfH_x are higher than those of HfD_x. The temperature dependence of thermal diffusivity changes significantly with changes in the composition of the samples, as the phase transformation is altered. The thermal diffusivities of δ′-phase $HfH_{1.48-1.53}$ at room temperature are higher than that of metallic α-Hf. At temperatures above 350 K, the thermal diffusivities for all the HfH_x and HfD_x samples are lower than that of α-Hf. In the case of δ′-phase HfH_x and HfD_x, the change in heat conduction is caused by the phase transformation from the δ′- to the δ-phase in the temperature range of 360–380 K. The effect of phase transformation on the thermal transport properties was confirmed through specific heat and electrical resistivity measurements.

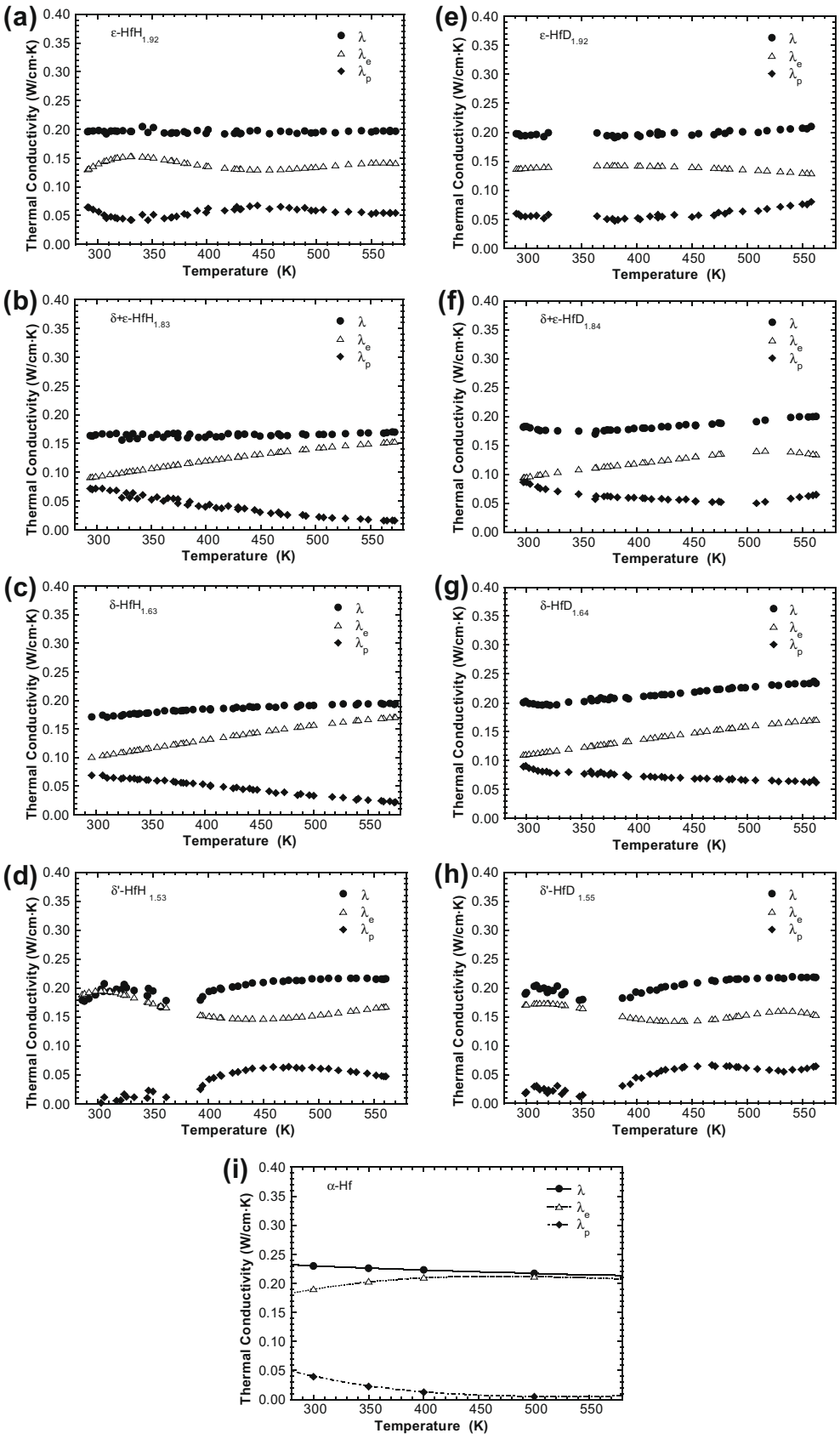

Fig. 8. Temperature dependence of the thermal conductivities associated with the migration of free electrons and phonons (λ_e, and λ_p, respectively) for (a) ε-$HfH_{1.92}$, (b) δ+ε-$HfH_{1.83}$, (c) δ-$HfH_{1.63}$, (d) δ′-$HfH_{1.53}$, (e) ε-$HfD_{1.92}$, (f) δ+ε-$HfD_{1.84}$, (g) δ-$HfD_{1.64}$, (h) δ′-$HfD_{1.55}$, and (i) α-Hf. λ represent the calculated thermal conductivity ($\lambda = \lambda_e + \lambda_p$).

In addition, the thermal conductivity of δ′-$HfH_{1.53}$, δ-$HfH_{1.63}$, δ+ε-$HfH_{1.83}$, ε-$HfH_{1.92}$ and δ′-$HfD_{1.55}$, δ-$HfD_{1.64}$, δ+ε-$HfD_{1.84}$, ε-$HfD_{1.92}$, obtained from the relationship between the measured thermal diffusivity, calculated density, and specific heat, was found

to be a function of temperature. The calculated thermal conductivities of HfH_x and HfD_x at 550 K are approximately in the range 0.17–0.22 W/cm K and 0.20–0.23 W/cm K, respectively; these values are similar to the thermal conductivity of α-Hf (0.21 W/cm K). On the basis of the Wiedemann–Franz rule, heat conduction due to the migration of electrons and phonons for each phase was distinguished by considering the calculated thermal conductivity, experimental data on electrical conductivity, and the Lorenz number corresponding to the electronic conduction. For δ-, δ+ε-, and ε-phase HfH_x and HfD_x, heat conduction due to electron migration significantly influences the thermal transport properties. In particular, electron migration significantly influences the thermal conductivity values of δ′-phase HfH_x and HfD_x at temperatures below 400 K. On the other hand, heat conduction due to phonon migration has a greater influence on the isotope effects on the thermal transport properties of HfH_x and HfD_x.

References

[1] K. Konashi et al., in: Proceedings of the ICAPP'06, Reno, USA, 2006.
[2] T. Nakagawa, S. Shibata, S. Chiba, T. Fukahori, Y. Nakajima, Y. Kikuchi, T. Kawano, Y. Kanda, T. Ohsawa, H. Matsunobu, M. Kawai, A. Zukeran, T. Watanabe, S. Igarashi, K. Kosako, T. Asami, J. Nucl. Sci. Technol. 32 (12) (1995) 1259.
[3] S.S. Sidhu, L. Heaton, D.D. Zauberis, Acta Cryst. 9 (1956) 607.
[4] S.S. Sidhu, Acta Cryst. 7 (1954) 447.
[5] S.S. Sidhu, J.C. McGuire, J. Appl. Phys. 23 (11) (1952) 1257.
[6] L. Espagno, P. Azou, P. Bastien, Compt. Rend. 250 (1960) 4352.
[7] R.K. Edwards, E. Veleckis, J. Phys. Chem. 66 (1962) 1657.
[8] M.H. Mintz, Hydrogen Metal Systems I, Hafnium-Hydrogen, 1996. p. 331 (Chapter 8).
[9] C.C. Weeks, M.M. Nakata, C.A. Smith, in: Proceedings of the 7th Conference on Thermal Conductivity, 13–16 November 1967, 1968, p. 387.
[10] Y. Arita, T. Ogawa, B. Tsuchiya, T. Matsui, J. Them. Anal. Cal. 92 (2008) 403.
[11] Y. Arita, K. Suzuki, T. Matsui, J. Phys. Chem. Solids 66 (2005) 231.
[12] M. Ito, K. Ko, H. Muta, M. Uno, S. Yamanaka, J. Alloys Comp. 446&447 (2007) 451.
[13] B. Tsuchiya, M. Teshigawara, K. Konashi, M. Yamawaki, J. Alloys Comp. 330&332 (2002) 357.
[14] Y.S. Touloukian, R.W. Powell, C.Y. Ho, M.C. Nicolaou, Thermophysical Properties of Matter, The TPRRC Data Series, Thermal Diffusivity, vol. 10, IFI/Plenum, New York, Washington, 1973.
[15] B. Tsuchiya, M. Teshigawara, K. Konashi, S. Nagata, T. Shikama, M. Yamawaki, J. Nucl. Sci. Technol. 39 (4) (2002) 402.
[16] J.D. Cox, D.D. Wagman, V.A. Medvedev, CODATA Key Values for Thermodynamics, Hemisphere, New York, 1989.
[17] M.T. Simnad, Nucl. Eng. Des. 64 (1981) 403.
[18] H.E. Flotow, D.W. Osborne, J. Chem. Phys. 34 (1961) 1418.
[19] W.J. Tomasch, Phys. Rev. 123 (1961) 510.
[20] Y.S. Touloukian, R.W. Powell, C.Y. Ho, P.G. Klemens, Thermophysical Properties of Matter, The TPRRC Data Series, Thermal Conductivity, vol. 1, IFI/Plenum, New York, Washington, 1970.
[21] B. Tsuchiya, S. Nagata, T. Shikama, K. Konashi, M. Yamawaki, J. Alloys Comp. 356&357 (2003) 223.